PAPER

Effect of high carbon incorporation in Co substrates on the epitaxy of hexagonal boron nitride/graphene heterostructures

IOP Publishing Nanotechnology
Nanotechnology 29 (2018) 035602 (9pp) https://doi.org/10.1088/1361-6528/aa9c58

Effect of high carbon incorporation in Co substrates on the epitaxy of hexagonal boron nitride/graphene heterostructures

Alireza Khanaki[1], Hao Tian[1], Zhongguang Xu, Renjing Zheng, Yanwei He, Zhenjun Cui, Jingchuan Yang and Jianlin Liu

Quantum Structures Laboratory, Department of Electrical and Computer Engineering, University of California, Riverside, CA 92521, United States of America

E-mail: jianlin@ece.ucr.edu

Received 12 September 2017, revised 7 November 2017
Accepted for publication 22 November 2017
Published 13 December 2017

Abstract

We carried out a systematic study of hexagonal boron nitride/graphene (h-BN/G) heterostructure growth by introducing high incorporation of a carbon (C) source on a heated cobalt (Co) foil substrate followed by boron and nitrogen sources in a molecular beam epitaxy system. With the increase of C incorporation in Co, three distinct regions of h-BN/G heterostructures were observed from region (1) where the C saturation was not attained at the growth temperature (900 °C) and G was grown only by precipitation during the cooling process to form a 'G network' underneath the h-BN film; to region (2) where the Co substrate was just saturated by C atoms at the growth temperature and a part of G growth occurs isothermally to form G islands and another part by precipitation, resulting in a non-uniform h-BN/G film; and to region (3) where a continuous layered G structure was formed at the growth temperature and precipitated C atoms added additional G layers to the system, leading to a uniform h-BN/G film. It is also found that in all three h-BN/G heterostructure growth regions, a 3 h h-BN growth at 900 °C led to h-BN film with a thickness of 1–2 nm, regardless of the underneath G layers' thickness or morphology. Growth time and growth temperature effects have been also studied.

Supplementary material for this article is available online

Keywords: hexagonal boron nitride, graphene, heterostructure, molecular beam epitaxy, cobalt substrate, epitaxial growth

(Some figures may appear in colour only in the online journal)

Introduction

As a two-dimensional (2D) material, hexagonal boron nitride (h-BN) possesses excellent properties including a high band gap energy (~5.9 eV), extremely flat surface (root mean square roughness <0.2 nm) and free of dangling bond or surface charge trap, excellent dielectric properties ($\varepsilon \approx 3$–4 and $V_{breakdown} \approx 12\,MV\,cm^{-1}$) and high chemical resistivity [1–5]. In addition, its complementary electronic properties and similar hexagonal lattice structure to graphene (G) and other 2D systems such as transition metal dichalcogenides have made h-BN an ideal candidate for all electronic devices where nanoscale supporting, insulating, capping, or gating layers are needed [6–8]. In particular, hexagonal boron nitride/graphene (h-BN/G) stacked layers have recently attracted much attention since such heterostructure system can be used not only to study fundamental physics of G, e.g., Hofstadter butterfly effect, but also to develop next-generation nanoelectronic devices with superior performances, e.g. tunneling devices [9–15].

So far, h-BN/G heterostructures have been mostly prepared by assembling G and h-BN layers exfoliated from highly ordered pyrolytic graphite and h-BN bulk crystals, respectively [16, 17]. Although these high-quality structures

[1] These authors contributed equally to this work.

made by mechanical exfoliation are the best to showcase the material characteristic and/or device performance, all epitaxial vertical heterostructures with controllable thickness, size and well-defined orientation are indispensable toward practical applications. On this matter, both chemical vapor deposition (CVD) and molecular beam epitaxy (MBE) have been used widely for the growth of h-BN/G heterostructures on different substrates, especially, transition metals [18–28]. For example, Liu *et al* demonstrated the CVD growth of h-BN/G stacks on Cu foil via a two-step process [18]. Gao *et al* also reported the CVD growth of vertically stacked h-BN/G heterostructures on Cu foil using temperature-triggered (>900 °C) chemical switching approach [19].

Among all transition metal substrates, Co benefits from having a high melting point temperature (1495 °C in 1 atm) which minimizes the amount of substrate evaporation during annealing step and high-temperature growth process. This is very crucial when a thin transition metal (foil or thin film) is used as a substrate, in particular, when a long growth duration is required for the 2D material growth, as this is often the case for h-BN and h-BN/G heterostructures. Also, metal substrates with a higher carbon (C) solubility such as Co (~1.5% at 900 °C) allow one to work with a wide range of C concentration and within a wide range of growth temperatures. For instance, in our group, we grew h-BN/G heterostructures with few-layer h-BN flakes and single-layer G with less than 1° miss-match angle [27] as well as continuous large-area few-layer h-BN and thick graphitic structure [28] based on Co substrates with different substrate surface conditions, growth temperature, growth time, and other growth parameters. A summary of recent advances on the growth of vertical h-BN/G heterostructures is provided in table S1 is available online at stacks.iop.org/NANO/29/035602/mmedia (supporting information).

Because many parameters such as source, substrate, growth pressure, growth temperature and substrate cooling rate play roles in the growth of these h-BN/G heterostructures, two major growth mechanisms, namely, precipitation growth and direct layer-by-layer epitaxy, have been observed. Nevertheless, to date, it is still challenging to precisely and reliably control the thickness, morphology and quality of h-BN and G layers, and their alignment across the wafer scale due to the complicated growth processes. In addition, either h-BN/G growth mechanism on the transition metal substrates or the effect of individual G or h-BN layers on each other's growth, morphology and thickness remains unclear. Therefore, to further elucidate the growth conditions for precise control of different types of h-BN/G heterostructures, in this paper, we systematically study the effect of high C incorporations in Co on the growth mode/morphology of the epitaxial h-BN/G heterostructures. Three different growth regions of h-BN/G heterostructures are identified based on the concentration of dissolved C atoms in Co and G growth mode. Moreover, the epitaxial relationship between the top h-BN film and bottom G layers in h-BN/G heterostructures is clarified.

Experimental details

Commercial Co foil (Alfa Aesar, 0.1 mm thick, 99.95% purity) was used as the substrate. As-received Co foils were polished by an SBT 920 Lapping and Polishing workstation. Then, Co foils were cut into 1 cm × 1 cm pieces, degreased with acetone and IPA, etched by diluted HCl solution (10%) for 2 min to remove the native oxides, and rinsed with deionized water. After blown-dry using a nitrogen gun, the fresh substrates were immediately loaded onto substrate holders and transferred to the growth chamber.

A plasma-assisted MBE (Perkin-Elmer) system was used for the sample growth. A Knudsen effusion cell filled with B_2O_3 powder (Alfa Aesar, 99.999% purity) was used as boron (B) source. Nitrogen plasma (Airgas, 99.9999% purity) generated by an electron cyclotron resonance (ECR) system and high-purity ammonia (American Gas Group, 99.9995% purity) were used as nitrogen (N) sources. Acetylene gas (C_2H_2, Airgas, 99.999% purity) was used as C source. The substrates were heated to 800 °C–950 °C and annealed at the growth temperature under a 10 sccm (standard cubic centimeters per minute) flow of hydrogen gas for 15 min. Then, at the same substrate temperature, 3 sccm acetylene gas was introduced into the chamber for a duration of 5 s ~ 3 min for different samples, and immediately after that, h-BN growth was started. During the growth, B cell temperature was maintained at 1150 °C; a mixture of nitrogen source consisting of N_2 gas flowed at 10 sccm through an ECR plasma generator and NH_3 gas leaked at a flow rate of 5 sccm through a needle valve was introduced into the chamber. The ECR current was set at 60 mA. The growth lasted from 15 min to 3 h for different samples. The substrate heating/cooling rate was ~10 °C min^{-1} for all samples. A schematic of the typical growth process is provided in figure S1 (supporting information).

Raman characterizations were performed using a HORIBA LabRam system equipped with a 60 mW, 532 nm green laser. Scanning electron microscopy (SEM) images were acquired using an FEI NNS450 SEM system in secondary electron mode. X-ray photoelectron spectroscopy (XPS) characterization was conducted using a Kratos AXIS ULTRA XPS system equipped with an Al Kα monochromatic x-ray source and a 165 mm mean radius electron energy hemispherical analyzer. The depth-profile XPS characterization was performed on a 3 × 3 mm^2 area of the sample using a 2 keV Ar ion beam sputter with an etching rate of 1 nm min^{-1}. Atomic force microscopy (AFM) images were obtained using a Veeco D5000 AFM system in tapping mode. TEM images and selected area electron diffraction (SAED) patterns were acquired using a FEI Tecnai12 system. TEM sample was prepared by picking a transferred h-BN/G film using a 200 mesh Cu grid covered with Quantifoil carbon film with orthogonal arrays of 1.2 μm diameter holes. The details about the transferring process can be found in supporting information.

Co(contact)/h-BN/G/Co(foil) two-terminal devices were fabricated by a standard photolithography and lift-off process. A Co layer of 50 nm was patterned as top square

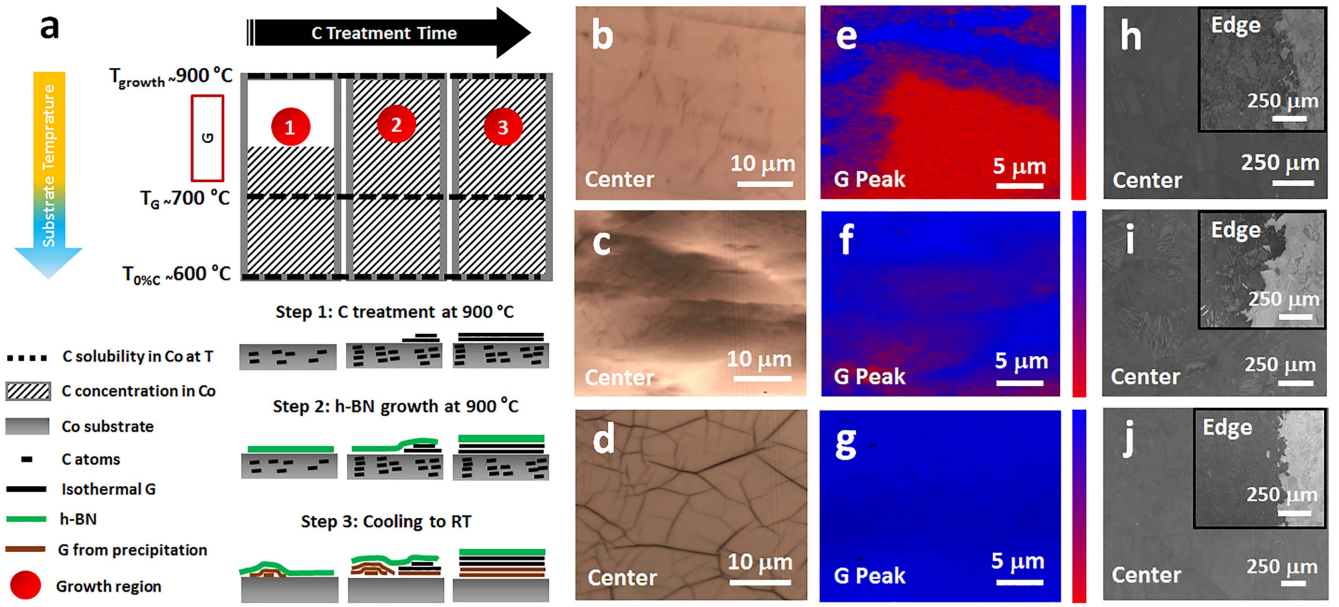

Figure 1. Growth regions of h-BN/G heterostructures on Co substrate. (a) Schematic of three h-BN/G growth regions with different C treatment time and same h-BN growth conditions (3 h at 900 °C). (b)–(d) OM images, (e)–(g) graphene G peak intensity mapping, and (h)–(j) SEM images of the samples with 30 s, 1.5 min, and 3 min C treatment time, which are representative samples in regions 1, 2, and 3, respectively.

contacts with an edge length of 25 μm on the surface of as-grown h-BN/G film. Current–voltage (I–V) characteristics were obtained by an Agilent 4155 C semiconductor parameter analyzer equipped with probing tips having a diameter of 5 μm (Signatone, SE-TL).

Results and discussion

Figure 1 summarizes the growth of the h-BN/G heterostructure system on the Co foil substrate when the C treatment time changes and h-BN growth conditions are the same (3 h at 900 °C). Note that C starts to dissolve in Co at around 600 °C ($T_{0\%C}$) and the solubility increases up to ~1.5% at 900 °C [29], i.e. a designated growth temperature (T_{growth}) in the schematic (figure 1(a)). The temperature-dependent growth of h-BN/G heterostructures indicated that the substrate temperature is an important growth parameter to influence the morphology and coverage of h-BN. With the same other growth conditions, a growth temperature window, which covers 900 °C, was identified for the formation of continuous high-quality h-BN films in the heterostructures as shown in figure S2 (supporting information). Thermodynamically, G growth on Co can start at a temperature of around or above 700 °C (T_G) [30, 31]. The black hatching areas in figure 1(a) show the C concentration in Co substrate at different growth regions (i.e., 1, 2, and 3), and the black horizontal dashed lines display the C solubility levels in Co substrate at designated temperatures (i.e., $T_{0\%C}$, T_G and T_{growth}). The growth regions in figure 1(a) are identified based on the C treatment time, and subsequently, G growth mode/morphology in the h-BN/G samples. Samples with 30 s, 1.5 min, and 3 min C treatment time are selected as representative samples for regions 1, 2, and 3, respectively, and their optical microscopy (OM), graphene G peak Raman intensity mapping, and SEM images are shown in figures 1(b)–(j).

Region 1 is where C solubility or saturation of Co is not reached at the growth temperature of 900 °C, hence, G is formed only by precipitation during substrate cooling process, leading to a 'G network' underneath the h-BN film. The dark regions in the OM image of figure 1(b) for a 30 s C sample and corresponding Raman intensity mapping of graphene G peak in figure 1(e) display the nature of the G network. Because of this specific morphology, G does not cover a big portion of the Co substrate surface in region 1 samples. This is related to the local accumulation of precipitated C atoms around edge areas of the h-BN flakes (i.e., grain boundaries) which is discussed in detail later. This morphology was observed when the C treatment time changed between 5 and 45 s.

Region 2 is where the Co substrate is just saturated by C atoms at the growth temperature and, therefore, a part of G growth now occurs isothermally via C saturation-precipitation mechanism [32–34]. Similar to region 1, another part of G growth in this region occurs later by precipitation when reducing the substrate temperature. Since in region 2 the isothermal G growth is limited only to the formation of a few G flakes/islands, a non-uniform G growth underneath h-BN film is obtained, as seen in the OM image of figure 1(c) for 1.5 min C treatment time sample and corresponding Raman intensity mapping of graphene G peak in figure 1(f). Despite the non-uniform morphology in region 2 samples, based on the Raman mapping results in figure 1(f), the G almost fully covers the Co surface. This was further verified by G reference sample where 1.5 min C treatment time was used to grow only G at 900 °C, as shown in figure S3 (supporting

information). This morphology was observed when the C treatment time changed between 45 s and 2 min.

Further introduction of C at the growth temperature with the C treatment time exceeding 2 min leads the growth mode into region 3. In this region, isothermally grown G has already covered the entire substrate surface at the growth temperature, and after the formation of continuous h-BN on the isothermally grown continuous G layer, additional G layers are formed under the structure during the cooling process, resulting in a uniform heterostructure consisting of thick G and thin h-BN (figures 1(d), (g), (j)) of the sample with 3 min C treatment time). Figure S4 (supporting information) shows OM image, graphene G peak Raman intensity mapping and typical Raman spectrum of the G reference sample with 3 min C treatment time. A 2D/G intensity ratio of ∼0.35 was calculated and no graphene D peak was observed in the spectrum (figure S4(d)), suggesting the high-quality growth of thick G layers. Figure S5 (supporting information) shows additional OM images of the h-BN/G samples to further illustrate the evolution of the G morphology in these three regions. Finally, in all three regions, h-BN is solely deposited at the growth temperature (a condition we referred as isothermally grown or epitaxial), i.e., it is not formed by precipitation mechanism during substrate cooling period. This is because the solubility of both B and N in Co are extremely low [35].

Figure 2 shows detailed characterization results of typical region 1 samples. In the SEM images of h-BN/G samples with 5-, 30- and 45 s C treatment time (figures 2(a)–(c)), distinct G network morphology appears with a darker color compared to the surrounding area as G produces less secondary electrons compared to the Co metal substrate [36]. The width of G network changes from 5 to 10 μm for 5 s C treatment time sample, to 11–13 μm for 30 s C treatment time sample, and to 12–16 μm for 45 s C treatment time sample. It seems that the width of G network increases notably from 5 to 30 s C treatment time and then remains about the same values from 30 to 45 s treatment time, which can be an indication of Co saturation by dissolved C atoms within 45 s of C treatment at the growth temperature of 900 °C.

To better understand the h-BN/G network morphology, we transferred the sample with 30 s C treatment time onto SiO_2/Si substrate and performed AFM measurement (figure 2(d)). The measured AFM line profile reveals that the h-BN film thickness is ∼2.1 nm and h-BN/G network is ∼12.4 nm, suggesting a G network thickness of ∼10.3 nm. Figures 2(e) and (f) show Raman spectra of h-BN and h-BN/G network areas (1) and (2), respectively, marked in the AFM image in figure 2(d). It can be clearly seen that the point (1) only shows the h-BN E_{2g} vibrational mode at ∼1367 cm^{-1} (figure 2(e)), while point 2 shows the co-existence of h-BN and multilayer G peaks (figure 2(f)) [25–28]. Raman results suggest that h-BN is continuous although G is not in the region 1 samples. Figures 2(g) and (h) show C1s, and B1s and N1s XPS spectra of a 30 s C treatment sample, respectively. C1s peak occurs at 284.6 eV indicating the existence of C sp^2 bonding of G layers [37, 38]. B1s and N1s exhibit energy positions at 190.4 eV and 397.7 eV, respectively, which is consistent with the reported values for XPS signals of h-BN [39, 40]. By using sensitivity factors from the instrument manufacturer and calculating the atomic % of each atom, the B/N ratio is 1.03, suggesting an almost equal composition of B and N elements.

Figure 2(i) shows an OM image of a C-only reference sample. To grow this sample, the Co foil substrate was heated up to 900 °C, treated with 30 s C exposure and then cooled to room temperature. As it can be seen in figure 2(i), the G morphology in the C reference sample is quite different with G morphology of h-BN/G sample with the same amount of C treatment time (figure 1(b)). This difference in G morphology is believed to be caused by the top h-BN film rather than the Co substrate because the density of the Co substrate grain boundaries and imperfection sites in both h-BN/G and G reference samples should be about the same and uniformly distributed across the substrate's surface. The fact that the G in region 1 samples is only formed by precipitation during the cooling process, that is after h-BN film growth, makes the G morphology affected by the h-BN film. The G network morphology is the outcome of preferential C atom precipitation in the vicinity of h-BN grain boundaries, which have a random distribution within the h-BN film. Figure S6 (supporting information) shows characterization results of the G reference sample in region 1 with 30 s C treatment time. Graphene G peak intensity mapping of the reference sample (figure S6(a)) shows a more uniform distribution of less intense G peak compared to that of h-BN/G sample with the same G growth conditions (figure 1(e)). This suggests that when there is no h-BN on top, precipitated C atoms tend to form larger and thinner domains. Also, a D peak at ∼1356 cm^{-1} with a FWHM of ∼34 cm^{-1} is shown (figures S6(b) and (c)), indicating a low-quality G growth in this region. Thus, the h-BN growth affects the G growth (quality/morphology/thickness) in region 1 samples since the G is formed after h-BN growth. On the other hand, as the G growth mode gradually changes from precipitation during cooling process to isothermal growth at high temperatures (i.e., regions 2 and 3), the effect of top h-BN film on the growth and morphology of underneath G layers becomes less evident.

Figure 3 shows characterization results of h-BN/G samples with the same 30 s C treatment time and different h-BN growth time. It can be seen in the SEM images of figures 3(a)–(d) that the coverage and size of the triangular h-BN flakes increases as the increase of h-BN growth time and the whole Co substrate surface is almost covered with h-BN as the growth time reaches ∼1 h. Figure 3(e) shows h-BN lateral growth speed as a function of growth time. The area of h-BN coverage is obtained by ImageJ software, as illustrated in figure S7 (supporting information) and the growth speed is defined as the area of coverage divided by the growth time. As seen from figure 3(e), the h-BN lateral growth rate is relatively high in the short h-BN growth period (∼2.5% min^{-1} at 15 min), and then gradually decreases to lower values as the growth progresses (∼1% min^{-1} at 1 h). This further justifies the continuous morphology of the h-BN films for all samples grown for 3 h. It should be noted that the SEM image in figure 3(a) and OM image in figure 3(f) of the

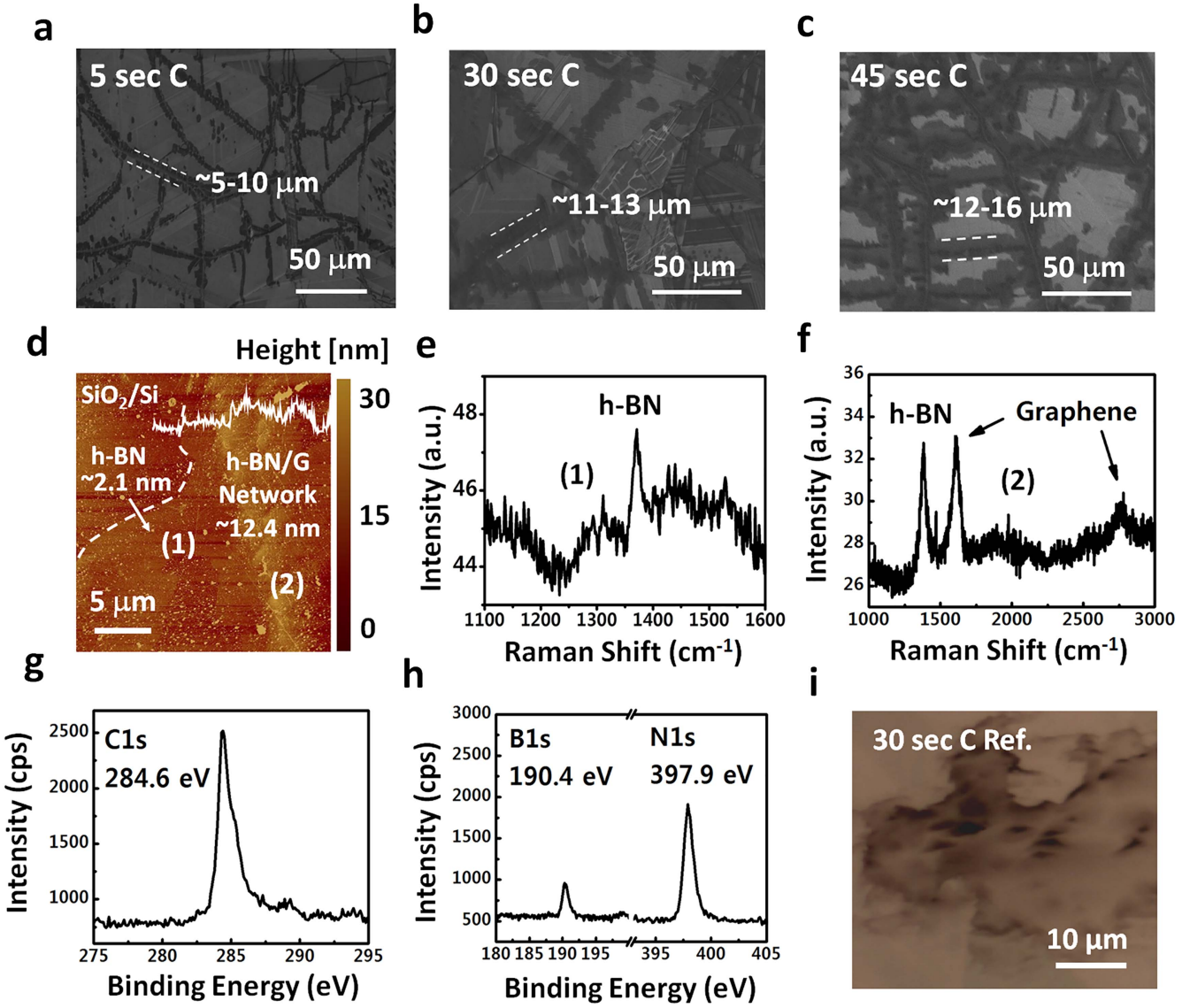

Figure 2. Characterizations of h-BN/G samples in region 1. SEM images of the h-BN/G samples with (a) 5 s, (b) 30 s, and (c) 45 s C treatment time showing the G network morphology. (d) AFM image of h-BN/G sample with 30 s C treatment time transferred onto SiO_2/Si substrate. (e) and (f) Raman spectra of the points (1) and (2) of (d), respectively. XPS signals of (g) C1s, and (h) B1s and N1s for as-grown h-BN/G sample with 30 s C treatment time. (i) OM image of the G reference sample with 30 s C time.

15 min h-BN growth sample show the accumulation of C atoms (dark color) around triangular h-BN flakes. Figures 3(g) and (h) show graphene G peak Raman intensity mapping of figure 3(f) and corresponding Raman spectra from the point of the strongest Raman signal in figure 3(g), respectively. The Raman scattering results clearly support the findings from the microscopy studies in figures 3(a) and (f). This behavior, i.e., C preferential precipitation along h-BN triangle edges and/or grain boundaries during the cooling process, is also consistent with the formation mechanism for the G network underneath the h-BN film of h-BN/G samples in region 1 (figures 1 and 2). The graphene 2D/G intensity ratio of the as-grown sample was calculated ~0.35 (figure 3(h)) which is much lower than that of G reference sample in region 1, namely ~0.6 (figure S6(b)). This further shows the effect of top h-BN film on the thickness of underneath G layers in region 1 samples. A wide FWHM of h-BN E_{2g} peak (~65 cm^{-1}) in figure 3(h) is due to the existence of intrinsic graphene D peak in the sample (figure S6(c)).

Figure S8 (supporting information) shows Raman spectrum and C1s, B1s and N1s XPS signals of a representative region 2 sample with a 1.5 min C treatment time, and AFM and OM images of the same sample after the h-BN/G structure was transferred onto a SiO_2/Si substrate and its corresponding h-BN E_{2g} phonon mode intensity mapping. Since the isothermal G growth in this region is limited only to the formation of a few G flakes/islands, the final G morphology in h-BN/G sample is a mixture of isothermal G growth and precipitation during the cooling process, resulting in a non-uniform G film. According to figure S8(f) (supporting information), despite the non-uniform morphology of G growth in this region, the h-BN has been formed continuously and fully covered the sample's surface.

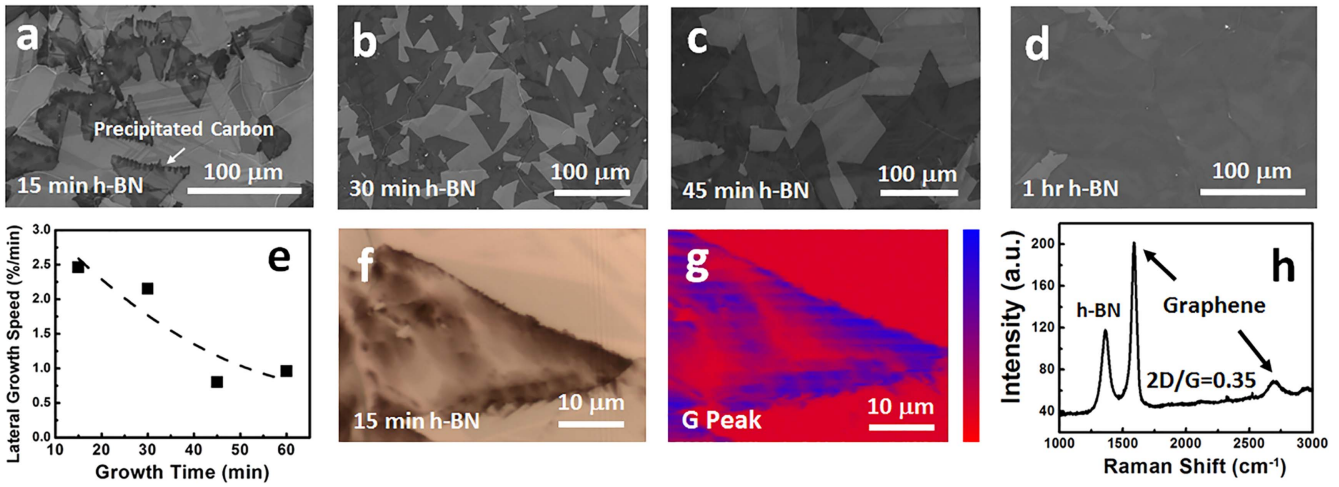

Figure 3. H-BN time-dependent growth of region 1 h-BN/G samples with 30 s C treatment time. (a)–(d) SEM images of h-BN/G samples with 15, 30, 45 min and 1 h h-BN growth duration. (e) h-BN lateral growth speed and triangle edge length for samples in (a)–(d). (f) OM image and corresponding (g) graphene G peak Raman intensity mapping and (h) Raman spectrum of (g) at its strongest signal point. H-BN E_{2g} Raman peak at ∼1367 cm^{-1} has a FWHM of ∼65 cm^{-1} and graphene 2D/G intensity ratio is ∼0.35.

Figure 4 shows characterization results of typical h-BN/G samples in region 3. Figure 4(a) shows Raman spectra of an as-grown h-BN/G sample with 3 min C treatment time at 13 locations across the 1 cm × 1 cm h-BN/G sample (indicated in a photo image in the inset of figure 4(a)). The existence of both multilayer G (MG or thin graphite) and h-BN Raman peaks is evident. The 2D/G ratio of MG in this sample was calculated ∼0.18. Figure 4(b) is the zoom-in spectra of figure 4(a) between 1200 and 1500 cm^{-1}, showing excellent uniformity of h-BN E_{2g} phonon mode's position (∼1366.5 cm^{-1}), intensity and full width at half maximum (FWHM ∼40 cm^{-1}) over these 13 points of measurement [41]. A portion of the sample was transferred onto SiO_2/Si substrate for the AFM measurement. The AFM image reveals that the h-BN/G film has a total thickness of ∼133 nm (figure 4(c)).

To reveal the individual thickness of h-BN and MG layers, we performed XPS sputtering depth profile measurement. Figures 4(d) and (e) show the evolution of C1s, and B1s and N1s XPS signals as a function of sputtering depth within 4 nm of the top surface of h-BN/G sample. As seen in figure 4(d), C1s peak is strongest when the sample was not sputtered, which is due to the inclusion of signals from absorbed C species on the surface or adventitious C [42]. After removing the top 0.17 nm material, the intensity of C1s peak drops significantly compared with the signal before sputtering and then remains about the same with further sputtering while the width of the C1s peak increases as the sputtering depth increases (down to ∼1–2 nm) due to Ar^+ beam induced damage. On the other hand, B1s and N1s XPS signals in figure 4(e) decrease proportionally and gradually by removing the top layers and become negligible when the sputtering depth reaches ∼2 nm (i.e., h-BN thickness). Figure 4(f) shows the calculated relative atomic concentration for B, N, and C as a function of the sputtering depth. As the sputtering depth increases, both N and B concentrations decrease gradually and reach an insignificant percentage at a sputtering depth of 1–2 nm, while the C concentration gradually levels up and then becomes steady as the etching depth extends from 2 to 4 nm. Considering the AFM (figure 4(c)) and XPS depth-profile (figure 4(f)) measurement results, it can be concluded that the h-BN/MG structure has a top h-BN layer of 1–2 nm and a bottom MG layer of 131–132 nm. Such a large thickness of MG is believed to be caused mainly by precipitation of dissolved C atoms during cooling process. Much higher substrate cooling rates could significantly reduce the total G thickness, although thermal strained induced wrinkles could compromise the quality of the precipitated G and/or h-BN in those cases [43]. Alternatively, other transition metals with much less C solubilities can be used to control the number of G layers down to a few layers [44, 45]. Owing to the fact that these C atoms precipitate underneath the isothermally grown MG buffer, the morphological and structural uniformity of h-BN/G samples is well preserved, as inferred from figures 1(c) and (g). Moreover, similar h-BN thickness in region 1 (∼2.1 nm) and region 3 (1–2 nm) samples indicates that the h-BN vertical growth is not affected by the G growth mechanism, morphology or thickness (figures 2 and 4). The seemly self-limited growth of h-BN on G with different morphology under the present growth condition is intriguing and needs further investigation. Similar self-limited growth of h-BN on metal substrates was also reported [46–50].

Figure 4(g) shows XRD pattern of the h-BN/G sample. The evident peaks at 26.64° and 54.79°, and 27.1° and 54.94° are assigned to (002) and (004) crystal plane diffractions of MG and h-BN films according to JCPDS card numbers 41-1487 and 34-0421, respectively [51, 52]. The small peak at 51.5° is from (002) crystal plane diffraction of hcp Co (JCPDS# 01-071-4239) [53, 54]. Such intense XRD peaks indicate the high quality of MG and h-BN films in the sample. It also suggests that h-BN and MG have grown along the same orientation. To further elucidate the growth relation between h-BN and MG, we transferred a piece of the same sample onto a Cu grid and

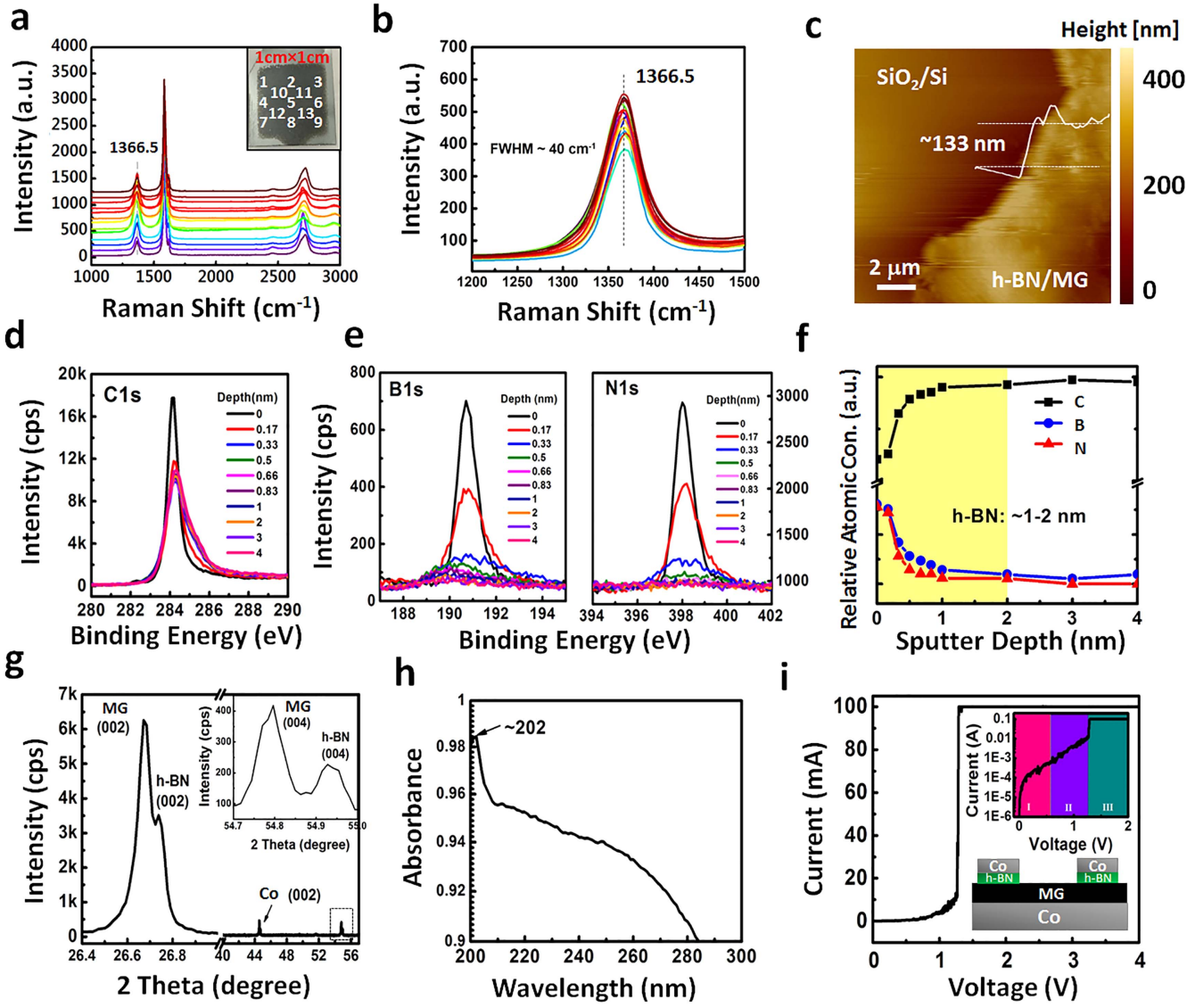

Figure 4. Characterization of h-BN/MG samples in region 3. (a) 13-points Raman spectra of the as-grown h-BN/MG sample with 3 min C treatment time and inset shows the sample photograph. The 2D/G ratio of G in this sample is ~0.18. (b) Zoom-in Raman spectra of (a) showing the h-BN E_{2g} phonon mode at ~1366.5 cm^{-1} with a uniform FWHM of ~40 cm^{-1} across these 13 points of measurement. (c) AFM image of the same sample transferred onto SiO_2/Si substrate with the total thickness of ~133 nm. (d) C1s and (e) B1s and N1s as a function of sputtering depth in the depth-profile XPS characterization and (f) relative atomic concentration of C, B, and N versus sputtering depth. (g) XRD spectrum of the same sample. Inset is the magnified spectrum with 2theta from 54.7° to 55°. (h) UV absorption spectrum of the h-BN/MG sample transferred onto a sapphire substrate. (i) *I–V* characteristic of Co(contact)/h-BN/MG/Co(foil) two-terminal device structure with the contact size of 25 μm × 25 μm. The inset displays the log-scale current versus voltage behavior of the device with 3 distinct regions.

performed TEM measurement (figure S9). Figure S9(a) shows a bright-field top-view image of the transferred film on the TEM grid, and figure S9(b) shows the SAED pattern obtained from the area in figure S9(a). A single hexagonal pattern is observed; however, the dots are slightly elongated, suggesting overlapping hexagonal patterns of h-BN and MG films with a negligible misalignment between each other. Figure 4(h) shows an absorption spectrum of the sample after a portion of the h-BN/MG film was transferred to a sapphire substrate. As can be seen in figure 4(h), the clear absorption edge at ~202 nm originates from the band gap of h-BN film [55]. A big portion of UV light spectrum has been also absorbed by the thick MG film [56]. Figure 4(i) shows cross-plane *I–V* characteristic of a Co(contact)/h-BN/G/Co (substrate) two-terminal device. The bottom inset shows a schematic of the device, which was fabricated using a process described in the Experimental section. The top inset displays the log-scale current versus voltage behavior of the device, showing 3 distinct regions: (I) current linearly increases as the increase of voltage, which represents direct-tunneling related conduction ($V < \sim 0.6$) [57, 58], (II) current nonlinearly/exponentially increases with the voltage under moderate biases ($\sim 0.6 < V < \sim 1.25$) due to the Fowler–Nordheim tunneling mode [59, 60], and (III) current sharply increases due to the dielectric breakdown at a bias of 1.25 V [61]. The calculated breakdown electric field based on an h-BN thickness of 1–2 nm is 6.25–12.5 MV cm^{-1}, which is comparable with the observed values from other epitaxial h-BN films [61–63].

Conclusion

We performed a systematic study of the *in situ* growth of h-BN/G films on a Co substrate by sequentially introducing a C source with a high C incorporation, and B and N sources in an MBE system. It is found that the continuous h-BN/G heterostructures can be formed at a substrate temperature of 850 °C–900 °C. By changing the C amount incorporation, the h-BN/G structure alters from region 1 where the G network is formed only by precipitation during cooling process underneath the h-BN film; to region 2 where isothermal G growth occurs to form G islands partially covering the substrate, followed by further precipitation G growth, leading to a non-uniform h-BN/G structure, and to region 3 where a uniform h-BN/G heterostructure with a thin continuous h-BN and a thick continuous MG are formed from both isothermal G growth and precipitation. It is found that the top h-BN film influences the morphology, thickness and quality of underneath G layers in h-BN/G samples of region 1. In addition, the h-BN growth is self-limited to a 1–2 nm thick film in all three regions, regardless of the underneath G thickness or morphology.

Acknowledgments

This work was supported in part by FAME, one of six centers of STARnet, a Semiconductor Research Corporation program supported by MACRO and DARPA.

ORCID iDs

Jianlin Liu https://orcid.org/0000-0001-6513-0867

References

[1] Nag A, Raidongia K, Hembram K P S S, Datta R, Waghmare U V and Rao C N R 2010 *ACS Nano* **4** 1539
[2] Liu L, Feng Y P and Shen Z X 2002 *Phys. Rev.* B **68** 104102
[3] Watanabe K, Taniguchi T and Kanda H 2004 *Nat. Mat.* **3** 404
[4] Hattori Y, Taniguchi T, Watanabe K and Nagashio K 2015 *ACS Nano* **9** 916
[5] Kim S M *et al* 2015 *Nat. Commun.* **6** 8662
[6] Novoselov K S A, Mishchenko A, Carvalho A and Castro Neto A H 2016 *Science* **353** 9439
[7] Xia W, Dai L, Yu P, Tong X, Song W, Zhang G and Wang Z 2017 *Nanoscale* **9** 4324
[8] Schulman D S, Arnold A J, Razavieh A, Nasr J and Das S 2017 *IEEE Nanotechnol. Mag.* **11** 6
[9] Yankowitz M, Xue J, Cormode D, Sanchez-yamagishi J D, Watanabe K, Taniguchi T, Jarillo-Herrero P, Jacquod P and LeRoy B J 2012 *Nat. Phys.* **8** 382
[10] Aggoune W, Cocchi C, Nabok D, Rezouali K, Belkhir M A and Draxl C 2017 *J. Phys. Chem. Lett.* **8** 1464
[11] Dean C R *et al* 2013 *Nature* **497** 598
[12] Cheng R *et al* 2017 *Appl. Phys. Lett.* **110** 173507
[13] Dean C R *et al* 2010 *Nat. Nanotechnol.* **5** 722
[14] Amet F, Williams J R, Garcia A G F, Yankowitz M, Watanabe K, Taniguchi T and Goldhaber-Gordon D 2012 *Phys. Rev.* B **85** 073405
[15] Britnell L *et al* 2012 *Science* **335** 947
[16] Novoselov K S, Jiang D, Schedin F, Booth T J, Khotkevich V V, Morozov S V and Geim A K 2005 *Proc. Natl Acad. Sci. USA* **102** 10451
[17] Pacile D, Meyer J C, Girit C O and Zettl A 2008 *Appl. Phys. Lett.* **92** 133107
[18] Liu Z, Song L, Zhao S, Huang J, Ma L, Zhang J, Lou J and Ajayan P M 2011 *Nano Lett.* **11** 2032
[19] Gao T, Song X, Du H, Nie Y, Chen Y, Ji Q, Sun J, Yang Y, Zhang Y and Liu Z 2015 *Nat. Commun.* **6** 6835
[20] Wu Q, Jang S K, Park S, Jung S J, Suh H, Lee Y H, Lee S and Song Y J 2015 *Nanoscale* **7** 7574
[21] Summerfield A *et al* 2016 *Sci. Rep.* **6** 22440
[22] Wofford J M, Nakhaie S, Krause T, Liu X, Ramsteiner M, Hanke M, Riechert H and Lopes J M 2017 *Sci. Rep.* **7** 43644
[23] Plaut A S *et al* 2017 *Carbon* **114** 579
[24] Driver M S, Beatty J D, Olanipekun O, Reid K, Rath A, Voyles P M and Kelber J A 2016 *Langmuir* **32** 2601
[25] Zheng R, Khanaki A, Tian H, He Y, Cui Y, Xu Z and Liu J 2017 *Appl. Phys. Lett.* **111** 011903
[26] Xu Z, Zheng R, Khanaki A, Zuo Z and Liu J 2015 *Appl. Phys. Lett.* **107** 213103
[27] Zuo Z, Xu Z, Zheng R, Khanaki A, Zheng J-G and Liu J 2015 *Sci. Rep.* **5** 14760
[28] Xu Z, Khanaki A, Tian H, Zheng R, Suja M, Zheng J-G and Liu J 2016 *Appl. Phys. Lett.* **109** 043110
[29] Ishida K and Nishizawa T 1991 *J. Phase Equilib.* **12** 417
[30] Zheng M *et al* 2010 *Appl. Phys. Lett.* **96** 063110
[31] Kassab L R P, Martinelli J R, dos Santos A D, Ribeiro S J L and dos Santos M V 2016 *Mater. Res.* **19** 669
[32] McCarty K F, Feibelman P J, Loginova E and Bartelt N C 2009 *Carbon* **47** 1806
[33] Baraton L, He Z B, Lee C S, Cojocaru C S, Châtelet M, Maurice J-L, Lee Y H and Pribat D 2011 *Europhys. Lett.* **96** 46003
[34] Hamilton J C and Blakely J M 1980 *Surf. Sci.* **91** 199
[35] Hu X, Björkman T, Lipsanen H, Sun L and Krasheninnikov A V 2015 *J. Phys. Chem. Lett.* **6** 3263
[36] Luo J, Tian P, Pan C-T, Robertson A W, Warner J H, Hill E W and Briggs G A D 2011 *ACS Nano* **5** 1047
[37] Ci L *et al* 2010 *Nat. Mat.* **9** 430
[38] Zheng R, Xu Z, Khanaki A, Tian H, Zuo Z, Zheng J-G and Liu J 2017 *Thin Solid Films* **627** 39
[39] Xu Z, Tian H, Khanaki A, Zheng R, Suja M and Liu J 2017 *Sci. Rep.* **7** 43100
[40] Tonkikh A A, Voloshina E N, Werner P, Blumtritt H, Senkovskiy B, Güntherodt G, Parkin S S P and Dedkov Y S 2016 *Sci. Rep.* **6** 23547
[41] Gorbachev R V *et al* 2011 *Small* **7** 465
[42] Barr T L and Seal S 1995 *J. Vac. Sci. Technol.* A **13.3** 1239
[43] Choi D S, Kim K S, Kim H, Kim Y, Kim T Y, Rhy S-H, Yang C-M, Yoon D H and Yang W S 2014 *ACS Appl. Mater. Interfaces* **6** 19574
[44] Zhao P, Kumamoto A, Kim S, Chen X, Hou B, Chiashi S, Einarsson E, Ikuhara Y and Maruyama S 2013 *J. Phys. Chem.* C **117** 10755
[45] Takesaki Y, Kawahara K, Hibino H, Okada S, Tsuji M and Ago H 2016 *Chem. Mat.* **28** 4583
[46] Orofeo C M, Suzuki S, Kageshima H and Hibino H 2013 *Nano Res.* **6** 335
[47] Shi Y *et al* 2010 *Nano Lett.* **10** 4134
[48] Jang S K, Youn J, Song Y J and Lee S 2016 *Sci. Rep.* **6** 30449
[49] Preobrajenski A B, Vinogradov A S and Mårtensson N 2005 *Surf. Sci.* **582** 21
[50] Morscher M, Corso M, Greber T and Osterwalder J 2006 *Surf. Sci.* **600** 3280

[51] Stobinski L, Lesiak B, Malolepszy A, Mazurkiewicz M, Mierzwa B, Zemek J, Jiricek P and Bieloshapka I 2014 *J. Electron Spectrosc. Relat. Phenom.* **195** 145
[52] Bhimanapati G R, Kozuch D and Robinson J A 2014 *Nanoscale* **6** 11671
[53] Chioncel F M and Haycock W P 2005 *Chem. Vap. Depos.* **11** 235
[54] Khanaki A, Xu Z, Tian H, Zheng R, Zuo Z, Zheng J-G and Liu J 2017 *Sci. Rep.* **7** 4087
[55] Zhang C, Zhao S, Jin C, Koh A L, Zhou Y, Xu W, Li Q, Xiong Q, Peng H and Liu Z 2015 *Nat. Commun.* **6** 6519
[56] Meng J H, Zhang X W, Wang H L, Ren X B, Jin C H, Yin Z G, Liu X and Liu H 2015 *Nanoscale* **7** 16046
[57] Simmons J G 1963 *J. Appl. Phys.* **34** 2581
[58] Lee G H, Yu Y J, Lee C, Dean C, Shepard K L, Kim P and Hone J 2011 *Appl. Phys. Lett.* **99** 243114
[59] Pandey S *et al* 2014 *Nanoscale* **6** 3410
[60] Ji Y *et al* 2016 *Appl. Phys. Lett.* **108** 012905
[61] Britnell L *et al* 2012 *Nano Lett.* **12** 1707
[62] Hui F, Pan C, Shi Y, Ji Y, Grustan-Gutierrez E and Lanza M 2016 *Microelectron. Eng.* **163** 119
[63] Hattori Y, Taniguchi T, Watanabe K and Nagashio K 2016 *Appl. Phys. Lett.* **109** 253111